

## Supporting Information

### Effect of long range order on intermolecular interactions in Organic Semiconductors: Zinc octa ethyl porphyrin molecular thin films model systems

A. Kumar,<sup>a,b</sup> D. Naumenko,<sup>a,&</sup> G. Rossi,<sup>c</sup> E. Magnano,<sup>a</sup> S. Nappini,<sup>a</sup> F. Bondino,<sup>a</sup> E. Segoloni,<sup>a</sup> L. Amidani,<sup>c,^</sup> F. d'Acapito,<sup>d</sup> F. Boscherini,<sup>c</sup> L. Barba,<sup>e</sup> E. Pace,<sup>f</sup> M. Benfatto,<sup>f</sup> S. Casassa,<sup>g</sup> and M. Pedio<sup>a</sup>

#### SI-1 Instrumentation, data acquisition and data analysis for GIXRD

The X-ray beam for GIXRD measurements was monochromatized at 1.0 Å. Bidimensional diffraction patterns were recorded with a 2M Pilatus silicon pixel X-ray detector (DECTRIS Ltd.) positioned perpendicular to the incident beam, at a distance of 100 mm for Ordered/Si, Semioordered/ITO and disordered/ITO and 140 mm for semioordered/Si, from the sample. Samples were aligned with the diffractometer axis with the help of a laser light. Zero incidence angle as well as sample quote in the beam have been estimated by means of direct beam absorption effect. Sample inclination of collected data ranged from  $-0.2^\circ$  to  $0.4^\circ$  with respect to the estimated zero incidence angle. The  $q$  range of the observed peaks spanned from about  $0.5 \text{ \AA}^{-1}$  to  $2.4 \text{ \AA}^{-1}$ . Indexing of the patterns was performed by means of Mercury and SimDiffraction software and showed the presence of a single polymorph, by which it was possible to index all the visible spots. Patterns were calibrated by means of a  $\text{LaB}_6$  660C NIST standard, observing an instrumental broadening less than  $0.09^\circ$  in the  $q$  range of interest. We did not employ any device to reduce the beam footprint on sample.

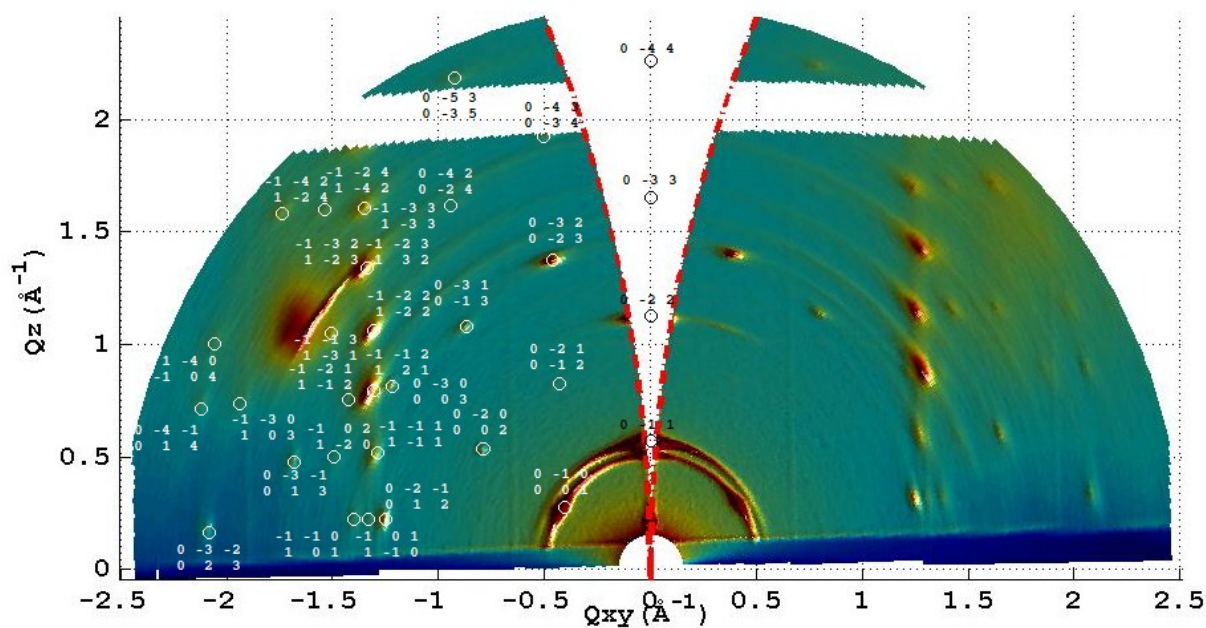


**Figure SI-1** Bidimensional diffraction pattern of the ZnOEP, Ordered/SiOx/Si thin films taken at  $0.04^\circ$  of incidence angle. Peaks were indexed by comparison with Mercury and SimDiffraction outputs from reported ZnOEP single crystal CIF.

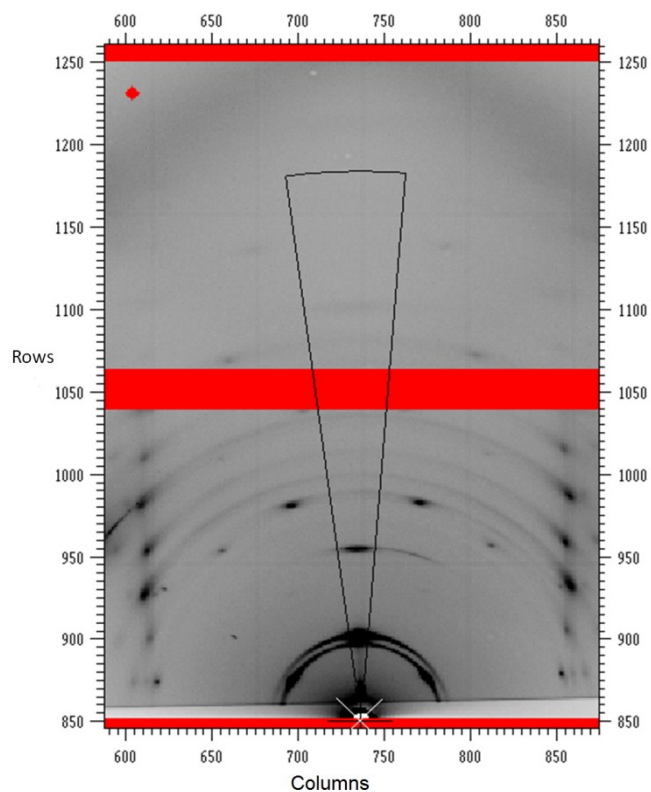


**Figure SI-2** Integration region along the out of plane (OOP) direction shown by thin line

Peak profile analysis was performed integrating the spots diffracted along the the (0 -1 1) direction, perpendicular to the substrate, by means of the Fit2D software (Fig. SI-2). They were extracted in a region of about 20° along Out of Plane (OOP) diffraction (0-1 1) direction, adjusted to minimize the background influence.

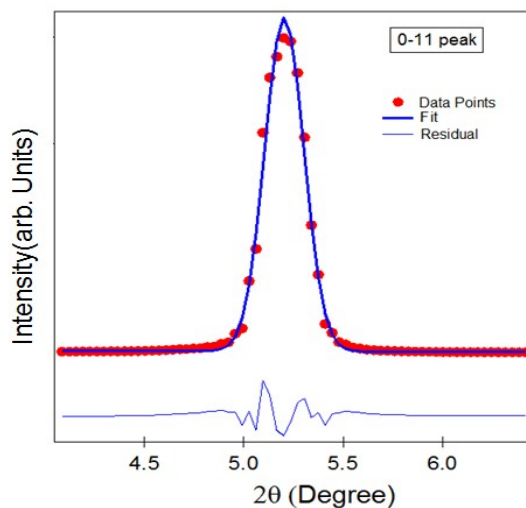


**Figure SI-3** Peak fitting using WinPlotr

2θ(Degree)	Estimated Standard deviation	d( Å)	Intensity	Estimated Standard deviation	FWHM	Estimated Standard deviation
5.2036	0.000069	11.0145	77855.79	53.11	0.2318	0.000124

**Table SI-1** Fit parameters corresponding to Figure SI-3 fit.

Peak profiles were fitted with WinPlotr (Fig. SI-3) in order to determine angular position and full width at half maximum (FWHM) of diffraction peaks which were employed as an input to the WAXX software, to calculate crystallite dimensions. The estimated standard deviations of the peaks FWHM were employed to estimate error bars on crystallite size. The output data for the four kind of samples are reported in Table SI1: The most relevant values are summarized in Tab. SI2. No instrumental broadening was included in WAXX input.

<b>Ordered/SiOx/Si</b>	<p>CRYSTALLITE SIZE RESULTS Wavelength : 1[Å]</p> <p>Profile nr. : 1 - [0-11] 2-Theta : 5.118464 deg HWHM : 0.110 deg - CGauss : .8 HWHM Strum. : 0.000 deg - CGauss Strum. : 0</p> <p>Profile nr. : 2 - [0-22] 2-Theta : 10.241371 deg HWHM : 0.141 deg - CGauss : .8 HWHM Strum. : 0.000 deg - CGauss Strum. : 0</p> <p>Profile nr. : 3 - [0-44] 2-Theta : 20.619844 deg HWHM : 0.228 deg - CGauss : .8 HWHM Strum. : 0.000 deg - CGauss Strum. : 0</p> <p>Average crystallite Size (surface weighted) &lt;D&gt;s : 218.0 [Å] Average crystallite Size (volume weighted) &lt;D&gt;v : 222.4 [Å]</p>	<b>Semiordered/SiOx/Si</b>	<p>CRYSTALLITE SIZE RESULTS Wavelength : 1[Å]</p> <p>Profile nr. : 1 - [0-11] 2-Theta : 5.203631 deg HWHM : 0.114 deg - CGauss : .8 HWHM Strum. : 0.000 deg - CGauss Strum. : 0</p> <p>Profile nr. : 2 - [0-22] 2-Theta : 10.259826 deg HWHM : 0.143 deg - CGauss : .8 HWHM Strum. : 0.000 deg - CGauss Strum. : 0</p> <p>Average crystallite Size (surface weighted) &lt;D&gt;s : 212.4[Å] Average crystallite Size (volume weighted) &lt;D&gt;v : 223.3 [Å]</p>
<b>Semiordered/ITO</b>	<p>CRYSTALLITE SIZE RESULTS Wavelength : 1[Å]</p> <p>Profile nr. : 1 - [0-11] 2-Theta : 5.196233 deg HWHM : 0.119 deg - CGauss : .8 HWHM Strum. : 0.000 deg - CGauss Strum. : 0</p> <p>Profile nr. : 2 - [0-22] 2-Theta : 10.339981 deg HWHM : 0.185 deg - CGauss : .8 HWHM Strum. : 0.000 deg - CGauss Strum. : 0</p> <p>Average crystallite Size (surface weighted) &lt;D&gt;s : 240.3 [Å] Average crystallite Size (volume weighted) &lt;D&gt;v : 247.3 [Å]</p>	<b>Disordered/ITO</b>	<p>CRYSTALLITE SIZE RESULTS Wavelength : 1[Å]</p> <p>Profile nr. : 1 - [0-11] 2-Theta : 5.041323 deg HWHM : 0.094 deg - CGauss : .8 HWHM Strum. : 0.000 deg - CGauss Strum. : 0</p> <p>Profile nr. : 2 - [0-22] 2-Theta : 10.107093 deg HWHM : 0.165 deg - CGauss : .8 HWHM Strum. : 0.000 deg - CGauss Strum. : 0</p> <p>Average crystallite Size (surface weighted) &lt;D&gt;s : 317.8 [Å] Average crystallite Size (volume weighted) &lt;D&gt;v : 292.8 [Å]</p>

**Table SI-2** WAXX output data for Peak Profile Analysis of samples deposited on Si with or without annealing (labeled ordered and semiordered) and on ITO with or without annealing (labeled semiordered and disordered).

Sample	GIXRD Average volume weighted crystallite size (nm)
Ordered/Si	22.40 ± 4.4
Semiordered/Si	22.33 ± 1.0
Semiordered/ITO	24.73 ± 0.7
Disordered/ITO	29.28 ± 3.8

**Table SI-3** Most relevant WAXX output values with estimated errors.

## SI-2 Power Spectral Density function in AFM results

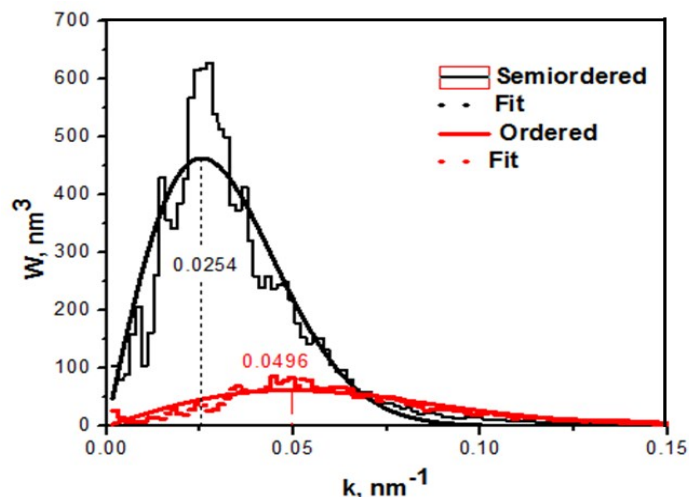


**Figure SI-4.** Power Spectral Density function derived from AFM images shown in Figure 2 (See Text). The peak position for the semiordered film (black curve) is close to one half the value for the ordered one and results in two times larger size of the surface crystallites. The AFM average grain size has been calculated by Gaussian fitting of Power Spectral Density function. The error has been estimated by standard deviation of Gaussian distribution.

## SI-3 Simulations of Raman spectra

Ab initio simulation of the Raman spectra of ZnOEP has been performed with the quantum-mechanic periodic CRYSTAL code<sup>1</sup>. Frequencies are obtained from the diagonalization of the mass-weighted Hessian matrix calculated with the hybrid functional B3LYP-D\* approach inclusive of dispersion interaction correction through the empirical D\* Grimme's term<sup>2</sup>. Relative intensities of the Raman peaks are determined through a fully analytical method<sup>3</sup> and powder spectra are obtained by computing integrals over all possible orientations of the optimized bulk crystal. To correct the well known overestimation of the observed ones, computed frequencies have been scaled using the factor 0.991, optimized for molecules within the adopted computational method.<sup>4</sup> Calculations were performed for three ZnOEP conformers: (a) isolated molecule in the initial configuration, (b) optimized molecule, and (c) the triclinic structure, as optimized by CRYSTAL at the B3LYP-D\* level.

	Initial configuration	Optimized	Triclinic Crystal
Zn-N	2.04	2.06	2.06
N-C <sub>α</sub>	1.38	1.37	1.37
C <sub>α</sub> -C <sub>m</sub>	1.40	1.39	1.39
C <sub>α</sub> -C <sub>β</sub>	1.45	1.45	1.45
C <sub>β</sub> -C <sub>1</sub>	1.51	1.50	1.50
C <sub>β</sub> -C <sub>β</sub>	1.38	1.37	1.37
C <sub>1</sub> -C <sub>2</sub>	1.53	1.54	1.54
C <sub>m</sub> -H	1.08	1.08	1.08
C <sub>1</sub> -H	1.11	1.09	1.09
C <sub>2</sub> -H	1.10	1.09	1.09

**Table SI-4** Bond distances in Å as obtained from the calculations.

Assignments	Experimental cm <sup>-1</sup> frequency (ordered film)	Calculated frequency cm <sup>-1</sup> (Frozen Molecule)
(C <sub>1</sub> C <sub>2</sub> )	1023	1038
(C <sub>α</sub> C <sub>β</sub> )	1139	1174
(C <sub>m</sub> H)	1210	1229
CH <sub>2</sub> twist	1257(weak)	1285
(C <sub>β</sub> C <sub>1</sub> H)	1320	1368
(C <sub>α</sub> N)	1376	1360
(C <sub>α</sub> N)	1404	1392
(C <sub>1</sub> H-C <sub>2</sub> H)	1492	1492-1511
(C <sub>β</sub> C <sub>β</sub> )	1561	1587
(C <sub>β</sub> C <sub>β</sub> )	1588	1615
(C <sub>α</sub> C <sub>m</sub> )	1621	1650

**Table SI-5** The assignments and the frequencies of Raman modes observed in the ordered film at 532 nm excitation wavelength.

## SI-4 EXAFS data reduction and analysis

Zn K-edge EXAFS spectra, measured at various sample orientations with respect to the linearly polarized x-ray beam ( $\theta$  being the angle between the sample plane and the x-ray wave-vector) were processed according to standard procedures using Athena<sup>5</sup>. The pre-edge region was fitted with a linear function while the post-edge region was fitted with a quadratic polynomial to simulate the atomic cross section. As a first approximation the energy origin for the energy to wavenumber conversion ( $E_0$ ) was chosen as the maximum of the first derivative of the absorption spectrum. The EXAFS functions obtained in this way are shown in Figure SI-5; the available  $k$  – range is relatively limited, due to the weak scattering amplitude of the light atoms and low effective density of metal ions.

The bulk EXAFS spectrum, was analyzed in the same  $k$  and  $R$  range as the TF samples for consistency. In order to understand the structural origin of the EXAFS signal, simulations in the MS framework were performed using the FEFF 6.0 code<sup>6</sup>. Atomic coordinates for ZnOEP in the triclinic crystallographic structure were used

as an input to generate SS and MS signals involving all atoms up to the 4<sup>th</sup> coordination shell. The EXAFS data of all samples were fitted using ARTEMIS<sup>1</sup>. The fitting range was  $k= 2.8-7.5 \text{ \AA}^{-1}$  and  $R=1.0-4.1 \text{ \AA}$ .

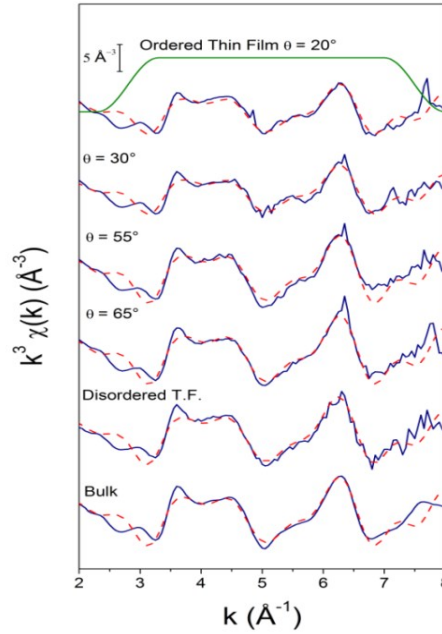


**Figure SI-5** Background subtracted  $k^3$  weighted EXAFS functions for bulk and TF samples (solid blue lines) with fit results (red dashed lines). The fitting window on the top is the same for all samples.

In order to correctly reproduce the experimental data relative to this peculiar system, an efficient and clear treatment of the damping of the signal due to thermal and structural disorder of single scattering (SS) and multiple scattering (MS) contributions is essential. We have based our approach on the work by Poiarkova and Rehr<sup>7</sup>. Overall, our analysis shows that the EXAFS spectrum of bulk ZnOEP can be confidently understood on the basis of a limited number of SS and MS paths, with reasonable local structural parameters. For a triangular MS path, the DW factor is the sum of the SS DW factors for two coordination shells and of a complex term  $C$  which takes into account dynamical correlations between shells. The DW factor for a fine structure signal due to  $n_{leg}$  scattering paths can be expressed as:

$$\sigma^2 = \frac{1}{4} \left\langle \left[ \sum_{i=1}^{n_{leg}} (\vec{u}_i - \vec{u}_i) \cdot \hat{R}_{ii} \right]^2 \right\rangle \quad (SI_1)$$

in which  $\vec{u}_i$  is the instantaneous displacement of the  $i$ -th atom from its equilibrium position,  $i'$  identifies the atom in the scattering path reached after atom  $i$ ,  $\hat{R}_{ii'}$  is the unit vector connecting the two atoms and  $\langle \rangle$  indicates a configurational average. For a SS contribution involving the central atom and atoms in the  $m$ -th and  $n$ -th shells we find the familiar expressions

$$\sigma_{m \text{ th shell}}^2 = \frac{1}{4} \langle [(\vec{u}_0 - \vec{u}_m) \cdot \hat{R}_{0m} + (\vec{u}_m - \vec{u}_0) \cdot \hat{R}_{m0}]^2 \rangle = \frac{1}{4} \langle [2 \cdot \frac{(\vec{u}_0 - \vec{u}_m) \cdot \hat{R}_{0m}}{\mathcal{A}}]^2 \rangle = \langle A^2 \rangle \quad (SI_2)$$

$$\sigma_{n \text{ th shell}}^2 = \frac{1}{4} \langle [(\vec{u}_0 - \vec{u}_n) \cdot \hat{R}_{0n} + (\vec{u}_n - \vec{u}_0) \cdot \hat{R}_{n0}]^2 \rangle = \frac{1}{4} \langle [2 \cdot \frac{(\vec{u}_0 - \vec{u}_n) \cdot \hat{R}_{0n}}{\mathcal{B}}]^2 \rangle = \langle B^2 \rangle \quad (SI_3)$$

For a triangular MS contribution involving the same atoms we obtain:

$$\sigma_{triangular}^2 = \frac{1}{4} \left[ \left( \frac{(\vec{u}_0 - \vec{u}_n) \cdot \vec{R}_{0n}}{\beta} + \frac{(\vec{u}_n - \vec{u}_m) \cdot \vec{R}_{nm}}{\beta} + \frac{(\vec{u}_m - \vec{u}_0) \cdot \vec{R}_{0m}}{\beta} \right)^2 \right] = \frac{1}{4} \langle (A + B + K)^2 \rangle = \frac{1}{4} \left( \langle A^2 \rangle + \langle B^2 \rangle + \frac{\langle K^2 \rangle + 2\langle AB \rangle + 2\langle AK \rangle + 2\langle BK \rangle}{\zeta} \right) = \frac{1}{4} \left( \sigma_{m^{th}Shell}^2 + \sigma_{n^{th}Shell}^2 + C \right) \quad (SI-4)$$

Path description	Geometry	Degeneracy	R <sub>0</sub> (Å)	Scattering angle
1 <sup>st</sup> shell SS	Zn-N-Zn	4	2.035	180°
2 <sup>nd</sup> shell SS	<b>Zn-C<sub>α</sub>-Zn</b>	8	3.055	180°
1 <sup>st</sup> -2 <sup>nd</sup> shell triangular MS	<b>Zn-N-C<sub>α</sub>-Zn</b>	16	3.228	126.6°
3 <sup>rd</sup> shell	<b>Zn-C<sub>m</sub>-Zn</b>	4	3.414	180°
4 <sup>th</sup> shell	<b>Zn-C<sub>β</sub>-Zn</b>	8	4.297	180°
1 <sup>st</sup> -4 <sup>th</sup> shell triangular MS	<b>Zn-N-C<sub>β</sub>-Zn</b>	16	4.321	162.7°

**Table SI-6** Most important paths, effective half length and scattering geometry. The C atom label corresponds to Figure 1 of the main section.

Parameter	Bulk	Disordered T.F	Ordered T.F
$\beta_{65^\circ}$	-	-	0.99 (0.13)
$\beta_{55^\circ}$	-	-	0.98 (0.14)
$\beta_{30^\circ}$	-	-	0.70 (0.11)
$\beta_{20^\circ}$	-	-	0.72 (0.10)
$\alpha (10^{-3})$	-1 (24)	0(15)	-1.1(5.8)
$\sigma_{1^{st}Shell}^2 (10^{-3} \text{ \AA}^{-2})$	3.4 (7.8)	3.2 (1.2)	3.2 (1.9)
$\sigma_{2^{nd}Shell}^2 (10^{-3} \text{ \AA}^{-2})$	7.1 (9.6)	6.7 (5.6)	7.2 (2.6)
$\sigma_{1^{st}-2^{nd}MS}^2 (10^{-3} \text{ \AA}^{-2})$	23 (73)	22 (44)	21 (24)
$\sigma_{3^{rd}Shell}^2 = \sigma_{4^{th}Shell}^2 (10^{-3} \text{ \AA}^{-2})$	15 (83)	16 (55)	13 (17)
$\sigma_{1^{st}-4^{th}MS}^2 (10^{-3} \text{ \AA}^{-2})$	0 (30)	2 (20)	0.0 (6.0)

**Table SI-7:** EXAFS fitting parameters

In order to fit the bulk sample, we found that only intra – molecular scattering paths due to in – plane atomic correlations were necessary to reproduce the spectrum. Six scattering paths, listed in Table SI-6, gave rise to signals of significant amplitude; this finding is in line with previous investigations on similar molecules<sup>8</sup>. A total of eight fitting parameters were used: the many – body amplitude reduction factor  $S_0^2$ , an energy origin shift  $\Delta E_0$ , an isotropic expansion coefficient  $\alpha$  which induces path length variations equal to  $\alpha R_0$  (in which  $R_0$  is the unmodified path length) and five DW factors. In order to reduce the number of fitting parameters and to obtain acceptable fits, the DW factors associated to the 3<sup>rd</sup> and 4<sup>th</sup> coordination shells were forced equal; other DW factors were those associated with the 1<sup>st</sup>, 2<sup>nd</sup> and 4<sup>th</sup> coordination shells and to the two triangular MS paths listed in Table SI-6.

Structural parameters obtained from the fitting procedure for the bulk sample are listed in the second column of Table SI-7 and fits are shown as the dashed lines in Figure SI-5. The parameter  $\beta$  is relevant only

for the TF samples and will be commented below. A good overall agreement is apparent. The estimates of the values of the local structural parameters are affected by rather large relative uncertainties, a consequence of the limited  $k$  – range; however, their values are reasonable since, in particular, the isotropic expansion factor is small and DW factors generally increase with increasing path length. An interesting observation is that  $\sigma_{1^{st}-2^{nd}MS}^2$  is significantly higher than  $\sigma_{1^{st}-4^{th}MS}^2$ ; in view of Eq. (SI\_4) this implies that the term  $C$  describing the correlation of motion between Zn, the 1<sup>st</sup> and 2<sup>nd</sup> shell atoms is large and positive while that involving Zn, the 1<sup>st</sup> and 4<sup>th</sup> shell atoms is negative. This is most likely related to the fact that  $\sigma_{1^{st}-4^{th}MS}^2$  is determined by two bond angle fluctuations while only one such term determines  $\sigma_{1^{st}-2^{nd}MS}^2$ .

The EXAFS spectra of the TF samples were fitted with the same contributions used for the bulk reference. The only difference was that, in order to empirically take into account the reduction of the EXAFS amplitudes, we introduced for each data set a multiplicative factor  $\beta$  for all paths. Since the sample orientation can influence only this amplitude factor, all the other parameters were set common for all data set. By fitting together all spectra taken with different orientations we found it possible to reduce dramatically the uncertainty on refined parameters. The fits are reported as the dashed lines in Figure SI-3 and the numerical values of the fitting parameters in Table SI-7. The overall quality of the fits is good and the values of the local structural parameters are close to those of the bulk reference.

### SI-5 Evaluation of the average molecular orientation from Zn K edge and N K edge near edge features

The normalized Zn K edge and N K edge XANES spectra of the ZnOEP TF are reported in Figure SI-6, showing the experimental spectra of the ordered sample taken at different grazing angles.

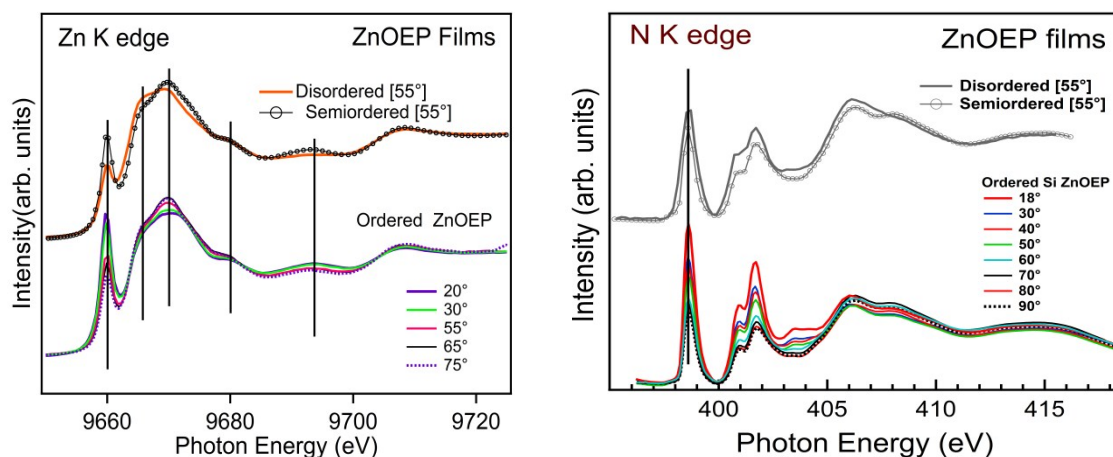


Figure SI-6. Normalized Zn K edge and N K edge XANES spectra of ZnOEP TFs.

The orientation of the LUMO with respect to the substrate can be quantified using the dichroic ratio,  $R$ , defined as

$$R = (I(90^\circ) - I(0^\circ)) / (I(90^\circ) + I(0^\circ)) \quad \text{SI-5}$$

where  $I(\Theta)$  indicates the intensity at an angle of incidence with respect to the surface plane, (as illustrated in Figure 6 in the text). For an azimuthally symmetric system, with the transition dipole tilted from the surface normal by an angle  $\theta$ ,

$$R = \frac{P(1 - 3 \langle \cos^2 \theta \rangle)}{2(1 - \langle \cos^2 \theta \rangle) - P(1 - 3 \langle \cos^2 \theta \rangle)}$$

Where P is the degree of polarization of the impinging beam,  $\approx 0.95$  in case of Zn K edge and 1 for N K edge. R can vary from 0.7, for a perfectly edge-on conjugated plane (for which no naturally occurring examples exist to our knowledge) to  $-1.0$  for a perfectly plane-on system (such as highly oriented pyrolytic graphite). An R of 0 is either consistent with a disordered orientation or a fixed magic-angle orientation of  $54.7^\circ$  away from surface normal ( $\langle \cos^2 \theta_m \rangle = 1/3$ ).

The measured trend of the dichroic ratio in N and Zn K edge measurements indicates that the  $\pi$  vector (that extends perpendicular to the conjugated plane of ZnOEP macrocycle) is preferentially oriented close to the normal to the substrate plane indicating that the molecular conjugated plane is preferentially oriented "plane-on" upon the substrate. This is confirmed by the negative values of the R factor (Figure SI-7).

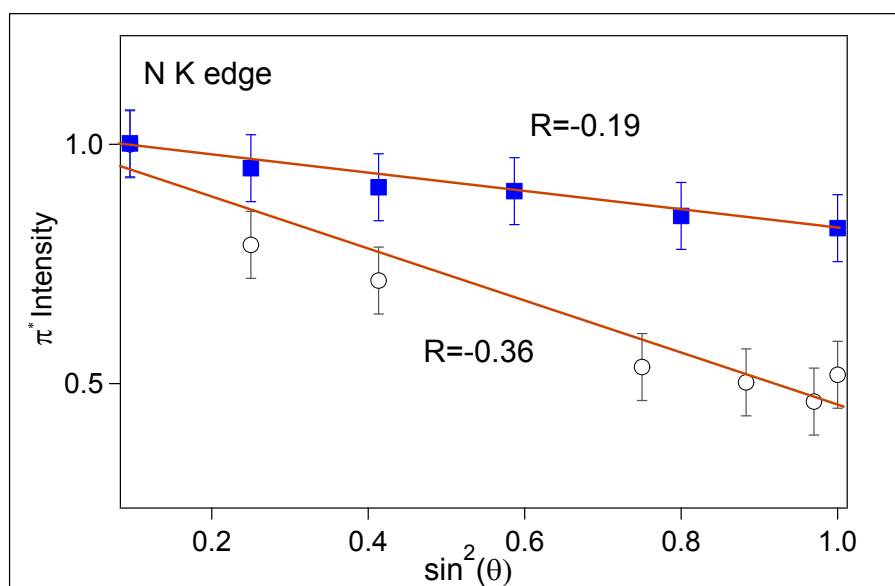


**Figure SI-7** Comparison of the LUMO intensity versus grazing angle for N K edges in the ordered (black point) and semioordered (blue squares) ZnOEP film. R is the dichroic ratio defined in eq. SI-5.

### SI-6 Fitting XANES procedure by MXAN

First of all, we performed a fit of the bulk spectrum in order to define the details of the potential. Then, the magic angle spectra of the films were fitted adopting the structural coordinates as fitting parameters. As a first attempt, the local structure derived from the EXAFS analysis were used, multiplied by the factor  $\beta$  reported in Table SI-7, up to the atoms at distances of about  $3.4 \text{ \AA}$  while the other coordinates were taken according to ref. 21. Then, two different coordinate models were used: the single molecule (SM Tr) of Fig. 1d, and the TR structural model consisting in the addition of the nearest C and N atoms (Figure 1 b) of the top and bottom ZnOEP molecules within the triclinic structure. Specifically, the coordinates of the  $C_\beta$ ,  $C_1$  and  $C_2$  atoms together with the nearest neighbor molecule atoms  $N_{up}$ ,  $N_{down}$ ,  $C_{\alpha \text{ up/down}}$ ,  $C_{m \text{ up/down}}$ , are taken as variables of the fit procedure, while the central N,  $C_\alpha$  and  $C_m$  atoms are fixed from the EXAFS analysis.

## SI-7 Instrumentation and data acquisition details for AFM and Raman Spectroscopy analyses

The Raman measurements were performed in the reflection geometry. A CW laser with a wavelength of 532 nm (Cobolt Samba, 50 mW, bandwidth 1 MHz) was used as excitation source. 532 nm RazorEdge Dichroic™ laser-flat beamsplitter and 532 nm RazorEdge® ultrasteep long-pass edge filter were used to direct the light into a microscope and to eliminate Rayleigh scattered light, respectively. The laser power on the sample was controlled by the neutral density filter (Thorlabs) and kept at 100 μW. The acquisition time in all experiments was 600 s. Atomic Force Microscopy (AFM) measurements were performed in contact mode using Nanowizard II AFM (JPK), which allows to scan the sample in the range of 100x100x15 μm. CSG 01 Silicon probes (NT-MDT) with a force constant of 0.05 N/m and 10 nm tip curvature were used.

## References

- 
- <sup>1</sup> R. Dovesi, V. R. S., C. Roetti, R. Orlando, C. M. Zicovich-Wilson, F. Pascale, B. Civalleri, K. Doll, N. M. Harrison, I. J. Bush, P. D'Arco, M. Llunell, M. Causà and Y. Noël. *CRYSTAL14 User's Manual*. University of Torino, Torino, (2014); R. Dovesi, R. Orlando, A. Erba, C.M. Zicovich-Wilson, B. Civalleri, S. Casassa, L. Maschio, M. Ferrabone, M. De La Pierre, Ph. D'Arco, Y. Noel, M. Causà, M. Rerat and B. Kirtman, *Int. J. Quantum Chem.* **114**, 1287 (2014).
  - <sup>2</sup> A. D. Becke, *J. Chem. Phys.* **98**, 5648 (1993); S. Grimme, *J. Comput. Chem.* **27**, 1787 (2006).
  - <sup>3</sup> L. Maschio, B. Kirtman, M. Rerat, R. Orlando, R. Dovesi, *J. Chem. Phys.* **139**, 164101 (2013).
  - <sup>4</sup> I. M. Alecu, J. Zheng, Y. Zhao, and D. G. Truhlar, *J. Chem. Theory Comput.* **6**, 2872 (2010).
  - <sup>5</sup> B. Ravel and M. Newville, *J. Synchrotron Radiat.* **12**, 537–541 (2005).
  - <sup>6</sup> S.I. Zabinsky, J.J. Rehr, A. Ankudinov, R.C. Albers and M.J. Eller, *Phys. Rev. B* **52**, 2995 (1995).
  - <sup>7</sup> A. V. Poiarkova, X-ray Absorption Fine Structure Debye-Waller Factors, Ph.D. dissertation, University of Washington (1999); A. V. Poiarkova and J.J. Rehr, *Phys. Rev. B* **59**, 948 (1999).
  - <sup>8</sup> G. Rossi, F. d'Acapito, L. Amidani, F. Boscherini, M. Pedio *Phys. Chem. Chem. Phys.*, **18**, 23686—23694 (2016).